

A Yellow-Emitting Homoleptic Iridium(III) Complex Constructed from a Multifunctional Spiro Ligand for Highly Efficient Phosphorescent Organic Light-Emitting Diodes

Bao-Yi Ren,^{†,‡,§,⊥} Run-Da Guo,^{||,⊥} Dao-Kun Zhong,^{†,⊥} Chang-Jin Ou,[§] Gang Xiong,[†] Xiang-Hua Zhao,[§] Ya-Guang Sun,^{*,†} Matthew Jurow,[‡] Jun Kang,[#] Yi Zhao,^{||} Sheng-Biao Li,^{*,||} Li-Xin You,[†] Lin-Wang Wang,[#] Yi Liu,^{*,‡} and Wei Huang^{§,⊥}

[†]Key Laboratory of Inorganic Molecule-Based Chemistry of Liaoning Province, College of Applied Chemistry, Shenyang University of Chemical Technology, Shenyang 110142, P. R. China

^{||}State Key Laboratory on Integrated Optoelectronics, College of Electronics Science and Engineering, Jilin University, Changchun 130012, P. R. China

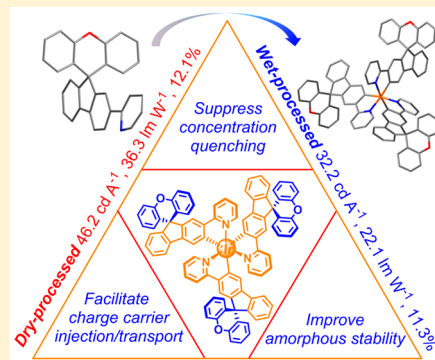
[‡]The Molecular Foundry and [#]Materials Science Division, Lawrence Berkeley National Laboratory, One Cyclotron Road, Berkeley, California 94720, United States

[§]Key Laboratory for Organic Electronics and Information Displays & Institute of Advanced Materials, Jiangsu National Synergetic Innovation Center for Advanced Materials, Nanjing University of Posts & Telecommunications, 9 Wenyuan Road, Nanjing 210023, P. R. China

[⊥]College of Chemistry, Central China Normal University, Wuhan 430070, P. R. China

Supporting Information

ABSTRACT: To suppress concentration quenching and to improve charge-carrier injection/transport in the emission layer (EML) of phosphorescent organic light-emitting diodes (PhOLEDs), a facial homoleptic iridium(III) complex emitter with amorphous characteristics was designed and prepared in one step from a multifunctional spiro ligand containing spiro[fluorene-9,9'-xanthene] (SFX) unit. Single-crystal X-ray analysis of the resulting *fac*-Ir(SFXpy)₃ complex revealed an enlarged Ir...Ir distance and negligible intermolecular π - π interactions between the spiro ligands. The emitter exhibits yellow emission and almost equal energy levels compared to the commercial phosphor iridium(III) bis(4-phenylthieno[3,2-*c*]pyridinato-*N,C*2')acetylacetonate (PO-01). Dry-processed devices using a common host, 4,4'-bis(*N*-carbazolyl)-1,1'-biphenyl, and the *fac*-Ir(SFXpy)₃ emitter at a doping concentration of 15 wt % exhibited a peak performance of 46.2 cd A⁻¹, 36.3 lm W⁻¹, and 12.1% for the current efficiency (CE), power efficiency (PE), and external quantum efficiency (EQE), respectively. Compared to control devices using PO-01 as the dopant, the *fac*-Ir(SFXpy)₃-based devices remained superior in the doping range between 8 and 15 wt %. The current densities went up with increasing doping concentration at the same driving voltage, while the roll-offs remain relatively low even at high doping levels. The superior performance of the new emitter-based devices was ascribed to key roles of the spiro ligand for suppressing aggregation and assisting charge-carrier injection/transport. Benefiting from the amorphous stability of the emitter, the wet-processed device also exhibited respectable CE, PE, and EQE of 32.2 cd A⁻¹, 22.1 lm W⁻¹, and 11.3%, respectively, while the EQE roll-off was as low as 1.7% at the luminance of 1000 cd m⁻². The three-dimensional geometry and binary-conjugation features render SFX the ideal multifunctional module for suppressing concentration quenching, facilitating charge-carrier injection/transport, and improving the amorphous stability of iridium(III)-based phosphorescent emitters.



INTRODUCTION

Phosphorescent organic light-emitting diodes (PhOLEDs) based on cyclometalated iridium(III) complexes have attracted enormous attention for their potential use in full-color flat-panel displays and solid-state light sources because of their ability to fully harvest both singlet (S) and triplet (T) excitons by strong spin-orbital coupling.¹⁻⁴ The high electroluminescent (EL) efficiency of iridium(III)-based emitters, attributable to their high intersystem-crossing yield from the lowest singlet

excited state (S₁) to the lowest triplet excited state (T₁), can reach unity because of the extraordinary heavy-atom effect of the centric Ir^{III} ion, thus laying the foundation for using cyclometalated iridium(III) complexes as dopants for highly efficient PhOLEDs.⁵⁻⁷ In the meantime, the intrinsic properties and EL performance of iridium(III)-based emitters, e.g.,

Received: April 28, 2017

emission color and efficiency, frontier molecular orbital (FMO) energy levels, suppression of the concentration quenching, and charge-carrier injecting/transporting ability, are closely dependent on the molecular structures of organic ligands coordinated to the Ir^{III} ions. Until now, it still remains a crucial problem for the PhOLEDs that the improvement of the device efficiency is often impeded by serious concentration quenching and triplet–triplet annihilation (TTA) because of strong intermolecular interactions of excited molecules, especially at high doping levels.^{8–10} Previously it has been demonstrated that the concentration quenching and TTA of iridium(III)-based phosphors can be relieved by the use of dendritic ligands possessing highly branched molecular structures. An important advantage of dendrimers is the presence of dynamic internal cavities, in which Ir^{III} ions can be comfortably embedded to give more protected metal centers. However, such ligands also suffer from laborious synthesis and troublesome purification.^{11–13}

Another feasible and effective approach to restraining the strong intermolecular interactions of iridium(III) emitters and to improve their spectroscopic and morphological stabilities is to introduce sterically hindered groups into the cyclometalated ligand. This approach can break the planarity of the cyclometalated ligand, while providing a dendrimer-like internal cavity for protecting the Ir^{III} centers, especially for homoleptic iridium(III) complexes.^{14,15} For instance, Che and co-workers initially demonstrated that self-quenching was significantly reduced for the iridium(III) complex in solution, even at very high concentration, because of the steric effect of the pinene spacer in the homoleptic iridium(III)-based emitter.¹⁶ As a result, a series of ligands with sterically hindered groups, such as alkyl,¹⁷ trimethylsilyl,¹⁸ cycloalkenyl,¹⁹ phenyl,^{20,21} 2,6-dimethylphenoxy,²² and diarylfluorene,²³ have been used to construct cyclometalated ligands for homoleptic or heteroleptic iridium(III) complexes. In particular, Wong and co-workers demonstrated that attaching arylamino units to the fluorene ring of the cyclometalated ligand can effectively decrease intermolecular interactions to afford iridium(III)-based phosphors with anti-TTA properties.^{24–26}

The common characteristics of steric groups in cyclometalated ligands are bulky, rigid, and nonelectroactive. An obvious disadvantage of nonelectroactive bulky moieties with steric hindrance effects, however, is the loss of luminance and emission efficiency with suppression of the concentration quenching.¹⁶ Hence, seeking multifunctionality beyond the steric effect is essential to overcoming the predicament for phosphorescent iridium(III) complexes.²⁷ The spiro aromatic skeleton has become a promising motif for constructing multifunctional steric-hindrance-type ligands. For example, the rigid spirobifluorene (SBF) with a three-dimensional (3D) orthogonal configuration was successfully introduced into the cyclometalated ligands, and the corresponding phosphorescent iridium(III) complexes showed satisfactory performances for PhOLEDs, attributable to the amorphous character of the dopants and controlled host–guest or guest–guest interactions.^{28,29} Benefiting from the convenient synthesis of spiro[fluorene-9,9'-xanthene] (SFX),³⁰ a heteronuclear analogue to SBF, we designed and synthesized a pyridine-appended bulky SFX ligand, 2-(spiro[fluorene-9,9'-xanthene])pyridine (SFXpy), for the phosphorescent platinum(II) complex, and the corresponding PhOLED devices showed a yellow emission peak at 548 nm, and no excimer emission or Pt⋯Pt interaction was observed in its EL spectra because of weakened intermolecular interactions of the emitter mole-

cules.³¹ In addition, the SFX-based derivatives were proven to be bipolar host materials with separated FMOs for high-performance PhOLEDs.³² Hence, relying on the interrupted and binary π systems of SFX, we anticipate that additional functions can be incorporated into the SFX-based ligands other than steric effects, including tuning the emission color, reducing aggregation, and assisting charge-carrier injection/transport for iridium(III)-based phosphorescent emitters.

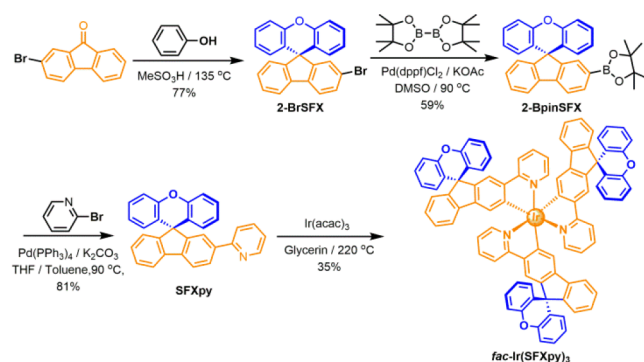
Yellow emission is one important chromaticity component to fulfill the requirement of a full-color display and to achieve the high-performance two-color (blue, yellow) white PhOLEDs. A series of yellow-emitting iridium(III) complexes have been developed,^{33,34} yet a detailed investigation of yellow-emissive iridium(III) complexes with SFX-based ligands remains absent. It is even more desirable to render the yellow-emissive iridium(III) emitters more compatible with both dry and wet processes, which are important for the low-cost, large-area manufacturing of high-performance devices.³⁵

In this contribution, a yellow-emitting homoleptic iridium(III) complex with a facial configuration was conceived and synthesized using SFXpy as the cyclometalated ligand. The steric structural features and optoelectronic properties were revealed on the basis of single-crystal X-ray crystallographic, photophysical, and electrochemical investigations. The yellow-emitting PhOLED devices were fabricated with different doping concentrations of the iridium(III) complex by dry and wet processes. As the doping concentration of the emitter was increased while keeping the same driving voltage, the current density increased accordingly, clearly indicating the iridium(III)-based emitter's capability of assisting charge-carrier injection/transport. The maximum device efficiency for dry-processed devices is superior to that for the control device fabricated using the commercial yellow emitter PO-01 as the dopant via vacuum thermal deposition, and for wet-processed devices, the efficiency is comparable to that of the control device. At the same time, such devices displayed low roll-off at high doping concentration, especially for the wet-processed device W2 with an EQE roll-off as low as 1.7% at a luminance of 1000 cd m⁻².

RESULTS AND DISCUSSION

Synthesis and Characterization. The SFXpy ligand and *fac*-Ir(SFXpy)₃ complex were prepared following the procedures described in Scheme 1. Using commercially available 2-bromofluorene and phenol as starting materials, the spiro skeleton of 2-BrSFX was facilely synthesized under acidic conditions. The sequential protocols of palladium-catalyzed

Scheme 1. Synthesis of the *fac*-Ir(SFXpy)₃ Complex



Miyaura borylation and Suzuki coupling were employed to afford the spiro ligand SFXpy (see the Supporting Information, SI, for the single-crystal X-ray crystallographic data of SFXpy). The final complex was synthesized by treating Ir(acac)₃ with SFXpy (3.4 equiv) in glycerol at 220 °C for 18 h. *fac*-Ir(SFXpy)₃ was obtained as a yellow powder after column chromatographic purification in a yield of 35%. The ¹H NMR spectrum of the complex reveals that the three ligands surrounding the Ir^{III} ion are magnetically equivalent, in keeping with the 3-fold molecular symmetry in a facial configuration. X-ray diffraction analysis of single crystals of the *fac*-Ir(SFXpy)₃ complex, obtained by the slow diffusion of hexane into its dichloromethane solution, clearly confirms its facial configuration. Details of the crystallographic data are summarized in Tables 1 and S1 and S2. As shown in Figure 1a, three SFXpy

Table 1. Crystallographic Data and Structure Refinement Information for *fac*-Ir(SFXpy)₃

identification code	CCDC 1482495
empirical formula	C ₉₀ H ₅₄ IrN ₃ O ₃
fw	1417.38
cryst syst	orthorhombic
space group	<i>Pbcn</i>
<i>a</i> (Å)	27.9461(7)
<i>b</i> (Å)	21.9877(5)
<i>c</i> (Å)	25.6824(5)
volume (Å ³)	15781.1(6)
<i>Z</i>	8
ρ_{calc} (g cm ⁻³)	1.543
μ (mm ⁻¹)	2.087
<i>F</i> (000)	7408.0
2 θ range for data collection (deg)	6.04–50.02
index ranges	–25 ≤ <i>h</i> ≤ 33, –26 ≤ <i>k</i> ≤ 25, –19 ≤ <i>l</i> ≤ 30
reflns collected	44760
indep reflns	13877 [<i>R</i> _{int} = 0.0459, <i>R</i> _σ = 0.0583]

ligands are coordinated to the central Ir^{III} ion to form a slightly distorted octahedral configuration with a *cis*-C,N chelate disposition, which is similar to the typical structural pattern of the *fac*-Ir(ppy)₃. Compared to the reported average C–Ir

and N–Ir bond lengths of the *fac*-Ir(ppy)₃ complex (2.042 and 2.084 Å, respectively),³⁶ the average bond lengths of C–Ir and N–Ir in *fac*-Ir(SFXpy)₃ are slightly altered to 2.016 and 2.117 Å, respectively. The nearest distance between two Ir^{III} centers in the crystal of *fac*-Ir(SFXpy)₃ is 10.996 Å, which is much larger than the corresponding distance in *fac*-Ir(ppy)₃ single crystals (7.701 Å) and the typical Ir–Ir bond length (ca. 2.6–3.1 Å) in multimetallic clusters, suggesting a lack of metal–metal interactions.^{36–39} The noncoordinating xanthene moiety of the ligand is nearly perpendicular to the plane of the chelating fluorene–pyridine unit. This renders the molecule highly sterically bulky, which is generally beneficial for reducing the concentration quenching of the emission.⁴⁰ The nearest centroid–centroid distance between the fluorene and xanthene rings is 4.28 Å (Figure 1b), which is longer than 3.8 Å, the upper bound of the π – π -stacking distance in metal complexes.⁴¹ The absence of intermolecular π – π interaction in the solid state of *fac*-Ir(SFXpy)₃ can thus be concluded, which is usually responsible for perturbing the energy levels of radiative transitions, altering the radiative lifetime (τ_r), decreasing the radiative relaxation quantum yield, and even generating metal-to-ligand–ligand charge-transfer transitions.^{28,42}

fac-Ir(SFXpy)₃ exhibits good solubility in common organic solvents, such as dichloromethane, ethyl acetate, chloroform, and toluene. The good solubility of *fac*-Ir(SFXpy)₃, derived from the deaggregation effect of the spiro SFXpy ligands, is favorable for solution-based device fabrication. Thermogravimetric analysis (TGA) of *fac*-Ir(SFXpy)₃ indicates a degradation temperature of 356 °C at 5 wt % weight loss, confirming its excellent thermal stability (see Table 2 and Figure S1a). On the other hand, the lack of any endothermic/exothermic peaks in the differential scanning calorimetry (DSC) curve indicates that no crystallization and glass transformation occurs during the heating/cooling cycle of *fac*-Ir(SFXpy)₃ (Figure S1b). Such thermal behavior is conducive for the formation of high-quality thin films by vacuum deposition.

Photophysical Properties. Figure 2 shows the absorption and photoluminescence (PL) spectrum of *fac*-Ir(SFXpy)₃ at room temperature and the PL spectra at 77 K. In the electronic spectra, the high-intensity absorption bands below 300 nm can be assigned to the spin-allowed ligand-centered $1\pi \rightarrow \pi^*$

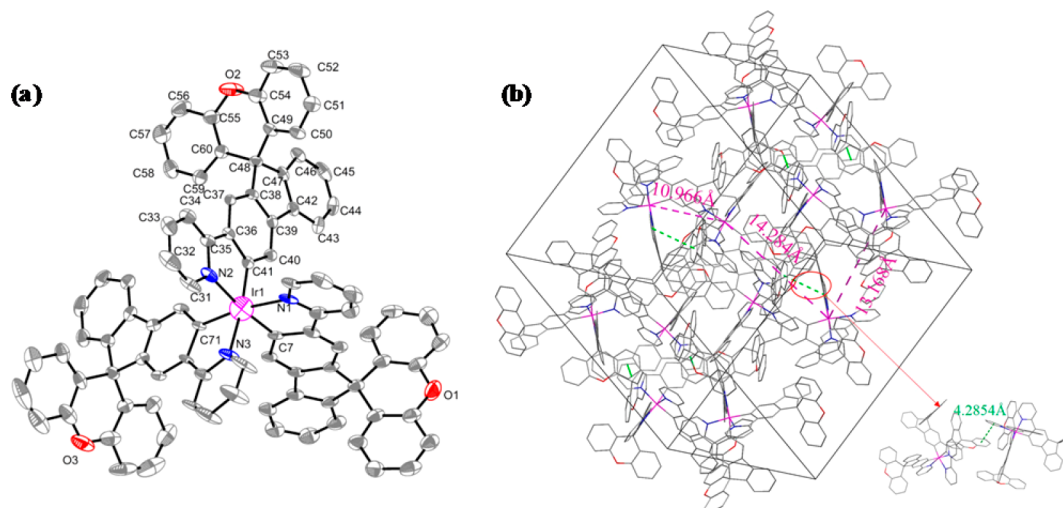


Figure 1. Crystal structure of *fac*-Ir(SFXpy)₃ with ellipsoids shown at the 40% probability level (a) and a representation of the crystal packing (b).

Table 2. Physical Properties for the *fac*-Ir(SFXpy)₃ Complex

complex	λ_{abs}^a (nm)	λ_{PL}^a (nm)	Φ_{p}^b (%)	τ_{p}^b (μs)	k_{r}^b (s^{-1})	T_{d}^c ($^{\circ}\text{C}$)	HOMO/LUMO ^d
<i>fac</i> -Ir(SFXpy) ₃	278, 303, 318, 334, 400	542, 580	18	0.11	5.56×10^5	356	-5.06 (-4.52)/-2.75 (-2.58)

^aMeasured in a CH₂Cl₂ solution (room temperature). ^bMeasured in degassed CH₂Cl₂; $\lambda_{\text{ex}} = 365$ nm. ^c T_{d} = decomposition temperature. ^dHOMO was calculated according to the formula $-[4.8 \text{ eV} + E_{\text{ox/red}} (\text{vs } E_{\text{Fc/Fc}^+})]$; the LUMO level was calculated from HOMO and $E_{\text{g}}^{\text{opt}}$. The data in parentheses are from theoretical calculations.

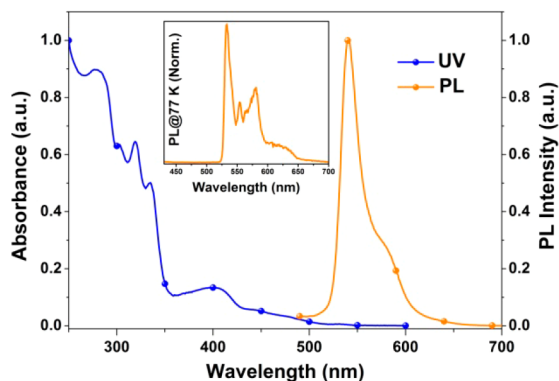


Figure 2. UV-vis absorption and PL spectra of *fac*-Ir(SFXpy)₃ in a CH₂Cl₂ solution at 298 K. The inset is the PL spectrum in degassed 2-methyltetrahydrofuran at 77 K.

intraligand charge-transfer transition. The absorption bands in the range of 300–350 nm arise from spin-allowed metal-to-ligand charge transfer (¹MLCT) mixed with an interligand charge transfer. The weaker and lower-energy bands above 350 nm are presumably from an admixture of the ³MLCT and the intraligand ³ $\pi \rightarrow \pi^*$ transitions, originating from the strong spin-orbit coupling of the *fac*-Ir(SFXpy)₃ complex. According to the absorption edge of *fac*-Ir(SFXpy)₃ at 537 nm, the optical energy gap ($E_{\text{g}}^{\text{opt}}$) was calculated to be 2.31 eV.⁴³ The emitter shows intense PL emission in a CH₂Cl₂ solution at a temperature of 298 K, with a strong emission peak located at 542 nm and a weak shoulder emission near 580 nm. Compared to the homoleptic analogue *fac*-Ir(ppy)₃, which has a PL peak at 494 nm in an ethanol/methanol solution at 77 K, the bathochromic shift in the PL spectra of *fac*-Ir(SFXpy)₃ can be attributed to the extended conjugation of the fluorene-pyridine moiety coordinated to a centric Ir^{III} ion.^{44,45} The triplet emission peak exhibits a large Stokes shift (ca.140 nm) from the lowest-energy absorption peak. At 77 K, the PL spectra of *fac*-Ir(SFXpy)₃ undergoes a pronounced rigidochromic shift and exhibits a well-resolved vibronically structured line shape between two major peaks, indicating that the mixing between the ³MLCT and ³ $\pi \rightarrow \pi^*$ levels is so effective that a ligand-centered emission can clearly be observed in the frozen matrix. The vibronic progression of ca. 1210 cm⁻¹ (ν_{0-1}) in the emission profile of *fac*-Ir(SFXpy)₃ corresponds to the aromatic stretching of the spiro ligand, which is diagnostic of the substantial involvement of the ligand-centered $\pi-\pi^*$ transition in PL.²⁶ Therefore, it suggests that the PL emission of the complex predominantly arises from the ligand-centered ³ $\pi \rightarrow \pi^*$ excited state.⁴⁶ The PL quantum yield (PLQY; Φ_{p}), measured in degassed CH₂Cl₂, is 0.18 for *fac*-Ir(SFXpy)₃ with a triplet lifetime (τ_{p} ; Figure S2) of ca. 0.11 μs at 298 K. Accordingly, τ_{r} of the triplet excited state, deduced from the equation $\tau_{\text{r}} = \tau_{\text{p}}/\Phi_{\text{p}}$, is 0.61 μs . The triplet radiative and nonradiative rate constants, k_{r} and k_{nr} , calculated from Φ_{p} and τ_{p} using the expressions $\Phi_{\text{p}} = \Phi_{\text{ISC}}[k_{\text{r}}/(k_{\text{r}} + k_{\text{nr}})]$ and $\tau_{\text{p}} = (k_{\text{r}} + k_{\text{nr}})^{-1}$, are 5.56×10^5 and 3.55×10^5 s⁻¹, where the

intersystem-crossing yield (Φ_{ISC}) is assumed to be 1.0 for iridium complexes because of the strong heavy-atom effect.^{7,47} The relatively high radiative rate constants, combined with the significantly shortened triplet lifetime, would be beneficial for high performance in devices because the triplet excitons can decay rapidly through the radiative pathway, while the TTA could be restrained simultaneously.⁴³

Electrochemical Properties and Theoretical Calculations. The electrochemical behavior of *fac*-Ir(SFXpy)₃ was investigated by cyclic voltammetry (CV) using a conventional three-electrode setup and the ferrocene/ferrocenium redox couple as an internal reference (Figure 3). The onset oxidation

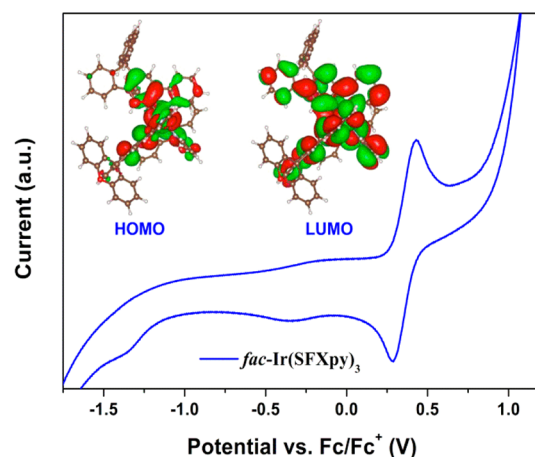
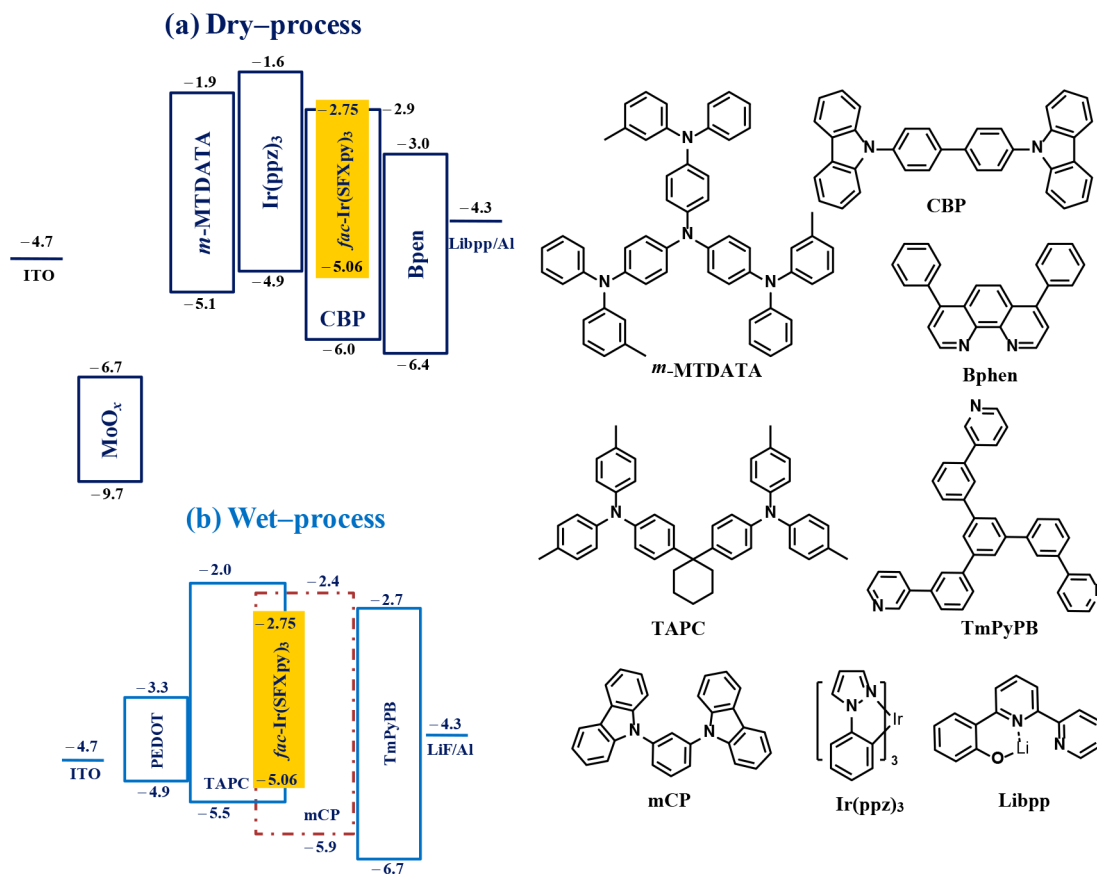


Figure 3. Cyclic voltammogram of *fac*-Ir(SFXpy)₃ in a chloroform solution. The insets are the calculated HOMO and LUMO orbital plots of the complex.

potential (E_{ox}) is 0.26 V with respect to Fc/Fc⁺, which can be attributed to the metal-centered Ir^{III}/Ir^{IV} oxidation couple.⁴⁸ Therefore, the highest occupied molecular orbital (HOMO) level is determined to be -5.06 eV. The lowest unoccupied molecular orbital (LUMO) level of -2.75 eV is estimated from the optical gap $E_{\text{g}}^{\text{opt}}$. For the well-known *fac*-Ir(ppy)₃, the corresponding HOMO and LUMO levels are -5.1 and -2.6 eV, respectively.⁴⁹ In comparison, *fac*-Ir(ppy)₃ possesses approximately the same HOMO level as that of *fac*-Ir(SFXpy)₃, while the LUMO is 0.15 eV lower in the more π -extended *fac*-Ir(SFXpy)₃. Interestingly, the HOMO and LUMO levels of *fac*-Ir(SFXpy)₃ are almost the same as those of the commercial emitter PO-01 (-5.1 and -2.7 eV for the HOMO and LUMO levels, respectively).^{50,51} For phosphorescent materials, the close FMO levels between two dopants usually signify that they possess similar charge-carrier injecting/transporting ability in an emission layer (EML) under the same configuration of PhOLED devices. Therefore, control devices using PO-01 as the dopant were fabricated for benchmarking the EL performance and the charge-carrier injecting/transporting abilities (vide infra).

Scheme 2. Configuration Diagrams of Dry- and Wet-Processed PhOLEDs Using *fac*-Ir(SFXpy)₃ as the Emitter and Structural Representations of Molecular Components



For a deeper understanding of the electrochemical behavior and FMO distribution of *fac*-Ir(SFXpy)₃, the 3D geometries were calculated based on the crystallographic structure of the molecule (computational details are described in the SI). The HOMO and LUMO surfaces of *fac*-Ir(SFXpy)₃ are plotted in Figure 3. The orbital distributions suggest that the HOMO is composed of a mixture of π orbitals of the coordinated phenylpyridine moiety and Ir^{III} d orbital (t_{2g}), and the LUMO is mainly distributed on the π orbital of the pyridine–fluorene moiety of the SFXpy ligand. The calculated HOMO and LUMO levels are -4.52 and -2.58 eV, respectively. Additionally, there are no FMOs located on the xanthene moiety of the ligand according to the calculated results, likely because of the interrupted linkage between the fluorene and xanthene rings by the spiro atom of SFX. Overall, the peripheral xanthene moiety imposes a steric effect on *fac*-Ir(SFXpy)₃, yet the latent capability of xanthene for hole transport should not be ignored.³² At the same time, shrinkage of the FMO energy levels and extended π system in the fluorene–pyridine conjugate should be favorable for charge-carrier injection/transport in *fac*-Ir(SFXpy)₃.

Dry-Processed OLEDs. To evaluate *fac*-Ir(SFXpy)₃ as the phosphorescent emitter, PhOLED devices were fabricated with the following configurations via vapor evaporation deposition: MoO_x (10 nm)/*m*-MTDATA (40 nm)/Ir(ppz)₃ (10 nm)/CBP:*x* wt % *fac*-Ir(SFXpy)₃ (10 nm)/Bphen (40 nm)/Libpp (3 nm)/Al (90 nm). Scheme 2 depicts the device configuration diagram and molecular structures of the layer components. Devices D1–D5 used a common host of 4,4'-bis(*N*-carbazolyl)-1,1'-biphenyl (CBP) with varying doping levels of

fac-Ir(SFXpy)₃ (D1–D5, in which $x = 5, 8, 12, 15,$ and 18 , respectively), where MnO_x and Libpp served as hole- and electron-injection layers, *m*-MTDATA and Bphen served as hole- and electron-transporting layers, and Ir(ppz)₃ was used as the hole-transporting and electron-blocking material, respectively.

The normalized EL spectra of these devices (Figure 4, at a driving voltage of 4.5 V) all showed a maximum emission peak located at 542 nm, together with a shoulder peak at 584 nm. There are no undesirable emission peaks from the host of CBP and the excimer of *fac*-Ir(SFXpy)₃, even at high operation

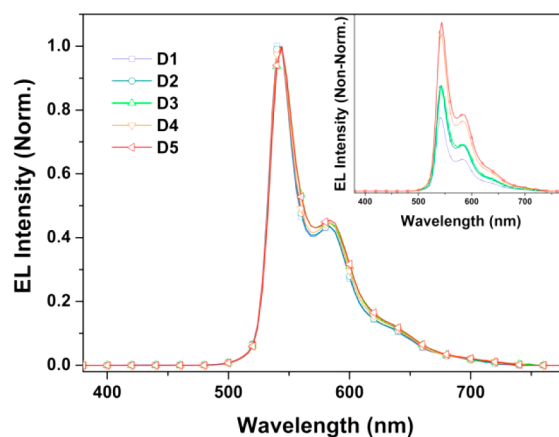


Figure 4. Normalized and non-normalized (inset) EL spectra of devices D1–D5 under a voltage of 4.5 V.

voltages (see Figure S3). The close resemblance between the EL and PL spectra suggests that the sufficient energy transfer from the host to the phosphor molecule in the EML is minimally affected by the doping concentration. Moreover, the non-normalized EL spectrum (inset in Figure 4) showed that the EL emission intensity gradually increased along with rising doping concentration. For devices D1–D5, the turn-on voltages are all at 2.8 V (Figure 5). It is worth noting that

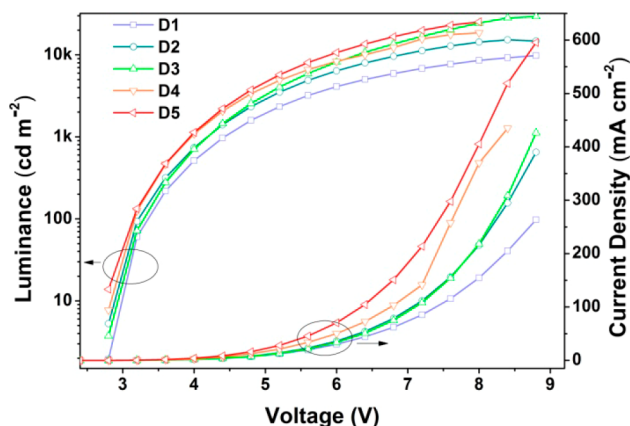


Figure 5. Current density (J)–voltage (V)–luminance (L) relationships of devices D1–D5.

the low driving voltages of 3.9–4.4 V of D1–D5 at a luminance of 1000 cd m^{-2} are favorable for the application of these devices in portable equipment (Figure 5 and Table 3). Similar to the doping concentration dependence trend observed for the EL intensity, the current densities of the devices increase as the doping concentration increases under the same driving voltage, which clearly indicates that the incorporation of *fac*-Ir(SFXpy)₃ facilitates both emission and charge-carrier injection/transport.⁵²

The influence of the doping concentration of *fac*-Ir(SFXpy)₃ on the device efficiency, specifically on the current efficiency (CE), power efficiency (PE), and external quantum efficiency (EQE), is shown in Figure 6 and summarized in Table 3. As the doping concentration changes from 5 to 8 wt %, the device efficiency increases and then levels off within the doping range between 8 and 15 wt %. The efficiency starts to drop upon a further increase of the doping concentration to 18 wt %. The device performances are maintained at high levels as $37.8\text{--}38.2 \text{ cd A}^{-1}$, $30.7\text{--}33.5 \text{ lm W}^{-1}$, and $9.5\text{--}10.2\%$ for CE, PE, and EQE, respectively, in the doping range of 8–15 wt %. It is quite

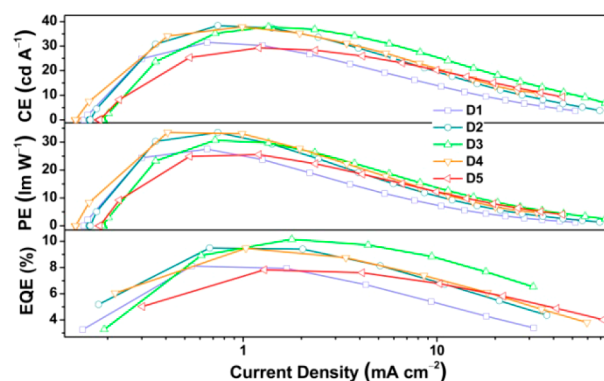


Figure 6. Efficiency curves of devices D1–D5.

remarkable that the devices show little self-quenching effect and high efficiency even at a high doping ratio of 15 wt %. Suppression of the concentration quenching can be attributed to the steric effect induced by the xanthene moiety to prevent clustering between the emitters. It is worth noting that the efficiency roll-off is relatively low in the high doping concentration range of 12–18 wt %. When the devices are compared at a luminance of 1000 cd m^{-2} , the PE of device D3 is 28.1 lm W^{-1} , corresponding to a roll-off of 8.5% (the maximum PE of D3 is 30.7 lm W^{-1}), while device D1 with a low doping level exhibits a PE of 18.7 lm W^{-1} , corresponding to a drastic roll-off of 32% (the maximum PE of D1 is 27.5 lm W^{-1}). Overall, the steric effect imposed by the xanthene unit in the phosphor guest can considerably reduce the concentration quenching, akin to previous reports using the uncoordinated fluorene moiety of SBF as the spacer in the framework of a phenylpyridine-type ligand.²⁸

In order to further survey the versatile roles of the *fac*-Ir(SFXpy)₃ emitter, the EML thickness was varied in devices D4 and D5 that have displayed high efficiency and low roll-off at high doping concentrations (15 and 18 wt %). Two devices with EML thickness of 20 nm, namely D4–2 and D5–2, were fabricated to study the effect of thicker EML layer on charge-carrier injection/transport and device performance (Figures 7 and 8). For comparison, a control device D-PO was fabricated using 6 wt % of the standard dopant PO-01, at which concentration peak efficiency was reported.^{53,54} For devices D4–2 and D5–2, the turn-on voltages are both about 3.0 V, which is slightly higher than that of devices D4 and D5 and attributable to the nearly doubled thickness of the EML, while the emission peak positions and CIE coordination still remain unchanged (see Figure S4). Among all of these dry-processed

Table 3. Summary of the EL Data of PhOLEDs

device	concn (wt %)	operation voltage ^a (V)	CE ^b (cd A ⁻¹)	PE ^b (lm W ⁻¹)	EQE ^b (%)	1931 CIE coordinates ^a	maximum luminance (cd m ⁻²)
D1	5	2.8/4.4	31.5/26.4	27.5/18.7	8.1/7.0	(0.41, 0.58)/(0.41, 0.58)	10018
D2	8	2.8/4.2	38.2/35.5	33.4/26.8	9.5/8.9	(0.41, 0.58)/(0.41, 0.58)	15147
D3	12	2.8/4.2	37.8/37.4	30.7/28.1	10.2/9.9	(0.42, 0.57)/(0.42, 0.57)	29254
D4	15	2.8/3.9	37.8/35.5	33.5/28.2	9.5/9.0	(0.42, 0.57)/(0.42, 0.57)	18443
D5	18	2.8/3.9	29.4/28.4	25.6/22.9	7.8/7.6	(0.42, 0.57)/(0.42, 0.57)	25170
D4–2 ^c	15	3.0/4.3	46.2/44.7	36.3/32.6	12.1/11.6	(0.42, 0.58)/(0.42, 0.58)	21048
D5–2 ^c	18	3.0/4.3	34.2/33.5	26.9/24.4	8.7/8.5	(0.42, 0.57)/(0.42, 0.57)	26788
D-PO ^c	6	3.2/5.1	33.1/28.4	24.2/17.8	9.5/8.0	(0.47, 0.52)/(0.47, 0.52)	14103
W1	4	3.6/5.0	30.2/29.9	20.2/18.7	10.6/10.4	(0.43, 0.52)/(0.43, 0.52) ^c	12860
W2	8	3.6/5.0	32.2/31.6	22.1/19.8	11.3/11.1	(0.40, 0.52)/(0.40, 0.52) ^c	13117

^aIn the order of at turn-on and at 1000 cd m^{-2} . ^bIn the order of at maximum and at 1000 cd m^{-2} . ^cIn the order of at maximum and at 6 V.

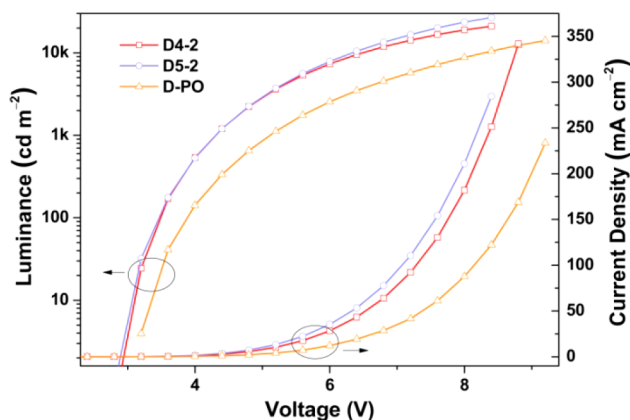


Figure 7. J - V - L relationships of devices D4-2, D5-2, and D-PO.

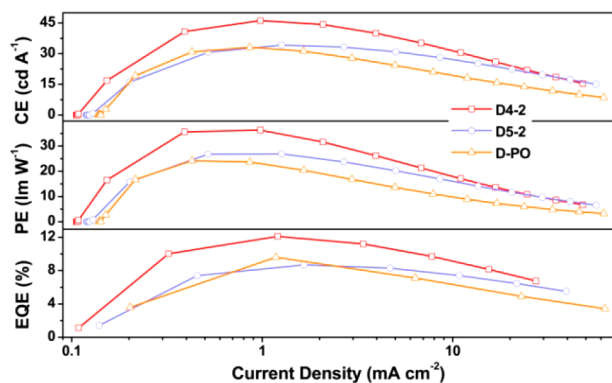


Figure 8. Efficiency curves of devices D4-2, D5-2, and D-PO.

devices, device D4-2 exhibits the highest CE, PE, and EQE of 46.2 cd A^{-1} , 36.3 lm W^{-2} , and 12.1%, respectively. Additionally, devices D4-2 and D5-2 possess lower roll-off compared to devices D4 and D5, indicating the effective suppression of self-quenching even at higher EML thickness. The reference device D-PO exhibited inferior device characteristics (CE, 33.1 cd A^{-1} ; PE, 24.2 lm W^{-2} ; EQE, 9.5%) and significant roll-offs of 14.2%, 26.5%, and 15.8% for the CE, PE, and EQE under a luminance of 1000 cd m^{-2} , respectively. In contrast to PO-01, *fac*-Ir(SFXpy)₃ has slightly shrunken FMO levels and extended π orbitals, which may be favorable for a more balanced electron and hole recombination in the EML.²¹ Together with the 3D spiro geometry of the *fac*-Ir(SFXpy)₃ emitter, the excellent performance of the devices could be attributed to the synergistic effects of the SFXpy ligand on charge-carrier injection/transport and on the intermolecular interactions between guest-guest/host-guest.

Wet-Processed OLEDs. The EL performance of *fac*-Ir(SFXpy)₃ was also tested in wet-processed PhOLEDs. The devices W1 and W2 were fabricated in the following configuration: ITO/PEDOT:PSS (20 nm)/EML (40 nm)/TmPyPB (60 nm)/LiF (0.8 nm)/Al (100 nm) (Scheme 2b). In the EML, the cohosts of TAPC and mCP were used in a weight ratio of 30:70, and the doping concentrations of the emitter were 4 and 8 wt % for devices W1 and W2, respectively. It should be noted that, for wet-processed OLEDs, the emitters are often doped into a polymer-based host matrix instead of a small molecular host matrix to avoid phase separation and ensure good film quality, which is often at the expense of the device performance.¹⁴ In the case when *fac*-Ir(SFXpy)₃ is employed as the emitter, the good amorphous stability of this

bulky emitter ensures excellent chemical compatibility with the small-molecule host, which allows the use of a small-molecule cohost matrix in the EML. The two wet-processed devices exhibit the same EL features as the peaks at 540 and 583 nm (Figure S5), which are also consistent with those of the dry-processed devices (Table 3). The turn-on and operation voltages at 1000 cd m^{-2} of the two devices are 3.6 and 5.0 V, respectively. The current density of the devices increases as the doping concentration is changed from 4 to 8 wt % (Figure 9).

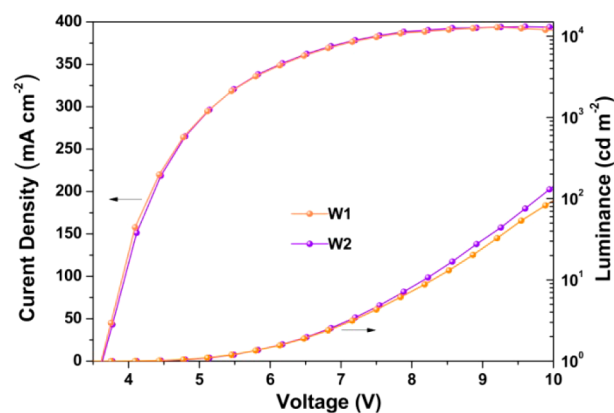


Figure 9. J - V - L relationships of devices W1 and W2.

In spite of an EML thickness of 40 nm, the charge-carrier injection/transport and energy transfer remain very efficient, as indicated by the J - V - L curves. Both devices W1 and W2 exhibit high performances, with device W2 showing a relatively superior efficiency (Figure 10 and Table 3). The slightly

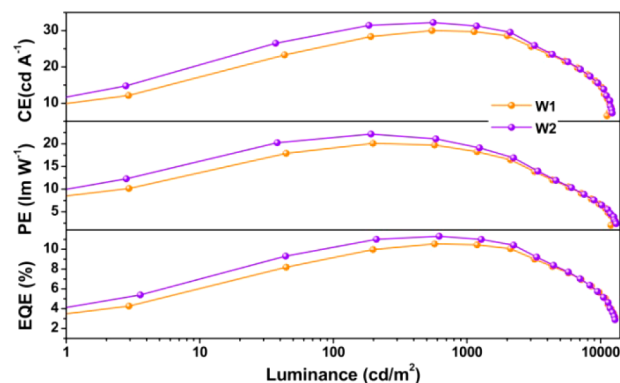


Figure 10. Efficiency curves of devices W1 and W2.

decreased PE and the relatively high operation voltage compared to the dry-processed devices may be due to the thicker EML in wet-processed devices. However, the high current efficiencies prove that the multifunctional feature of *fac*-Ir(SFXpy)₃ remains effective in promoting charge-carrier injection/transport in the wet-processed devices. Remarkably, under a luminance of 1000 cd m^{-2} , the EQE roll-off of device W2 is as low as 1.7%, which stands out from all of the reported wet-processed yellow PhOLEDs.³³ These results collectively demonstrate that the SFX-based ligand endows the *fac*-Ir(SFXpy)₃ emitter with good solution processability while suppressing the concentration quenching by evenly distributing the Ir^{III} dopant in the EML.

It can be found that the dry- and wet-processed devices show different efficiency roll-off behaviors; the wet-processed devices

possess lower roll-off than the dry-processed devices, especially at high luminance. As reported recently,⁵⁵ the emitter molecules tend to form networks in a vacuum-deposited EML, even at doping concentrations as low as 5 wt %, and percolated networks form through the entire EML as the doping concentrations are slightly increased. Such networks of emitter molecules in a vacuum-deposited EML, which is different from the even distribution of emitter guests in a solution-processed EML, would improve charge-carrier transport, but it could also give rise to more nonradiative pathways for the emissive state as well as a resultant loss of efficiency. In our cases, the maximum efficiencies of dry-processed devices stay on a high level in the doping range between 8 and 15 wt %, and the improved charge-carrier transport was observed simultaneously. This phenomenon suggests efficient blocking of the nonradiative pathways using these sterically hindered SFXpy ligands. The roll-offs of wet-processed devices are even lower. For further elucidating such low roll-offs of wet-processed devices, we measured the phosphorescent lifetimes of spin-coating films that blend *fac*-Ir(SFXpy)₃ into mCP at doping concentrations of 5, 10, and 20 wt % (Figure 11). The

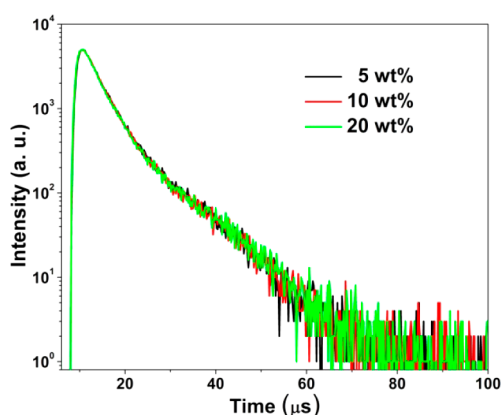


Figure 11. Phosphorescent lifetime (excited at 365 nm) curves under 298 K for spin-coating films blended *fac*-Ir(SFXpy)₃ with mCP at doping concentrations of 5, 10, and 20 wt %.

corresponding lifetimes are 5.54, 5.55, and 5.74 μ s, respectively. Additionally, the lifetime of *fac*-Ir(SFXpy)₃ in a neat film is 672 ns under the same measurement conditions (Figure S14). The transient lifetime dependence on the average distance between iridium(III) complexes (*R*) and the concentration-quenching rate constant are shown to be dependent on R^{-6} .⁵⁶ Therefore, the tiny change of the transient lifetimes of solid film samples with different doping concentrations indicates that a spiro-functionalized SFXpy ligand effectively weakened the intermolecular interaction of *fac*-Ir(SFXpy)₃ emitters. These results collectively demonstrate that the SFX-based ligand endows the *fac*-Ir(SFXpy)₃ emitter with good solution processability while suppressing the concentration quenching by evenly distributing the Ir^{III} dopant in the EML.

CONCLUSIONS

In summary, a SFX-based ligand, SFXpy, was incorporated in a robust homoleptic iridium(III) complex, *fac*-Ir(SFXpy)₃, following simple synthetic procedures. Single-crystal X-ray analysis confirmed the facial configuration, elongated Ir \cdots Ir distance (no less than 11 Å), and negligible intermolecular π - π interactions of adjacent ligands in the crystal. The complex

shows yellow emission ($\lambda_{\text{max}} = 542$ and 580 nm, respectively) with a significantly shortened τ_p value of about 0.11 μ s and FMO energy levels (HOMO = -5.06 eV; LUMO = -2.75 eV) similar to those of the commercial emitter PO-01. In dry-processed devices using the common CBP host material and varying doping levels of *fac*-Ir(SFXpy)₃, the devices with high doping levels exhibit excellent device performance. The peak efficiencies of vacuum-deposited devices are 46.2 cd A⁻¹, 36.3 lm W⁻¹, and 12.1% for CE, PE, and EQE, respectively, at a doping concentration of 15 wt % with a 20-nm-thick EML. The devices kept high efficiencies and low roll-offs within the doping concentration range between 8 and 15 wt %. Furthermore, the wet-processed devices also exhibited excellent performance, with maximum efficiencies of 32.2 cd A⁻¹, 22.1 lm W⁻¹, and 11.3% for CE, PE, and EQE, respectively, at a doping concentration of 8 wt %, as well as a very low EQE roll-off of 1.7%. Compared with the control device using PO-01 as the emitter, *fac*-Ir(SFXpy)₃-based devices show a superior performance as yellow-emitting PhOLEDs. The EL performance studies of both dry- and wet-processed devices indicate that the SFXpy ligand endows *fac*-Ir(SFXpy)₃ with good amorphous stability and effective suppression of the concentration quenching while facilitating charge-carrier injection/transport in the devices. The research illustrates that SFX is a versatile module for building multifunctional cyclometalated emitters, whose unique structural features incorporating steric considerations may open the door to a more informed search for better-performing PhOLED materials.

EXPERIMENTAL SECTION

General Information. The solvents were dried using standard procedures, and all other reagents were used as received from commercial sources, unless otherwise stated. NMR spectra were recorded on a Bruker Avance500 II. The ¹H NMR chemical shifts (δ) of the signals were given in ppm and referenced to residual protons in the deuterated solvents: chloroform-*d*₁ (7.26 ppm). Mass spectrometry was recorded on an AB SCIEX TF4800 matrix-assisted laser desorption/ionization time-of-flight (MALDI-TOF) spectrometer. UV-vis-near-IR (NIR) spectra were recorded using a UV-3150 Plus UV-vis-NIR spectrophotometer. PL spectra were recorded using a RF-5301PC spectrofluorophotometer. Absolute PLQYs measured in CH₂Cl₂ were recorded on a FLS920 spectrometer with a xenon light source (450 W) through the Edinburgh Instruments integrating sphere. The integrating sphere is 150 mm in diameter and has its inner surface coated with barium sulfate (BaSO₄). The excited-state lifetime data were analyzed using F900 software by minimizing the reduced function (χ^2) and visual inspection of the weighted residuals. CV was performed using a 273A potentiostat (Princeton Applied Research), wherein glassy carbon, platinum, and a silver wire act as the working, counter, and pseudoreference electrode, respectively. Samples were prepared in a CHCl₃ solution with tetrabutylammonium hexafluorophosphate (0.1 M) as the electrolyte at a scan rate of 100 mV s⁻¹, using a ferrocene/ferrocenium (Fc/Fc⁺) redox couple as an internal standard. The HOMO and LUMO energy levels (eV) of the two compounds are calculated according to the formula $-[4.8 \text{ eV} + E_{\text{ox/red}} (\text{vs } E_{\text{Fc/Fc}^+})]$. DSC analyses were performed on a Shimadzu DSC-60A instrument. TGA was conducted on a Shimadzu DTG-60H thermogravimetric analyzer under a heating rate of 10 °C min⁻¹ and a nitrogen flow rate of 50 cm³ min⁻¹.

2-BrSFX. A mixture of 2-bromo-9H-fluoren-9-one (2.00 g, 7.70 mmol, 1 equiv), phenol (4.32 g, 46.3 mmol, 6 equiv), and methanesulfonic acid (2.0 mL, 2.96 g, 30.8 mmol, 4 equiv) was heated at 150 °C under nitrogen for 12 h. The reaction mixture was then slowly added into water (25 mL) and extracted with dichloromethane. The combined extracts were dried over MgSO₄, evaporated, and purified by column chromatography to afford the

product as a colorless solid (2.45 g, 77%). ^1H NMR (500 MHz, CDCl_3): δ 7.77 (d, $J = 7.6$ Hz, 1H), 7.66 (d, $J = 8.1$ Hz, 1H), 7.49 (dd, $J = 8.1$ and 1.8 Hz, 1H), 7.38 (t, $J = 7.5$ Hz, 1H), 7.28 (d, $J = 1.7$ Hz, 1H), 7.25–7.14 (m, 6H), 6.80 (ddd, $J = 8.2$, 6.4, and 2.1 Hz, 2H), 6.39 (d, $J = 7.5$ Hz, 2H).

2-BpinSFX. 2-BrSFX (1.50 g, 3.65 mmol, 1 equiv), bis(pinacolato)diboron (1.02 g, 4.01 mmol, 1.1 equiv), 1,1'-bis-(diphenylphosphino)ferrocene dichloropalladium(II) (148 mg, 0.18 mmol, 0.05 equiv), potassium acetate (713 mg, 7.30 mmol, 2.0 equiv), and dimethyl sulfoxide (30 mL) were placed in a flask, and the mixture was stirred for 5 h under a nitrogen atmosphere at 80 °C. After the reaction mixture was cooled to room temperature, water was added, the reaction mixture was transferred to a separation funnel, and the mixture was extracted with chloroform. The organic layer was concentrated under reduced pressure, and the concentrate was purified by silica gel column chromatography (hexanes/chloroform) to afford 2-BpinSFX (0.98 g, 59%). ^1H NMR (500 MHz, CDCl_3): δ 7.89 (d, $J = 7.6$ Hz, 1H), 7.83 (d, $J = 7.9$ Hz, 2H), 7.60 (s, 1H), 7.37 (d, $J = 7.5$ Hz, 1H), 7.25–7.15 (m, 6H), 6.77 (t, $J = 8.3$ Hz, 2H), 6.39 (d, $J = 7.9$ Hz, 2H), 1.31 (s, 12H).

SFXpy. A mixture of 2-BpinSFX (0.98 g, 2.14 mmol, 1 equiv), 2-bromopyridine (0.37 g, 2.35 mmol, 1.1 equiv), $\text{Pd}(\text{PPh}_3)_4$ (136 mg, 0.12 mmol, 0.05 equiv), K_2CO_3 (2.0 M aqueous solution, 2.5 mL), and toluene (15 mL)/tetrahydrofuran (15 mL) was stirred at 90 °C for 24 h. After it was cooled to room temperature, 50 mL of CHCl_3 was added to the reaction mixture. The organic portion was separated and washed with brine before drying over anhydrous MgSO_4 . The solvent was evaporated off, and the solid residue was purified by column chromatography on silica gel to afford SFXpy as a white solid (0.71 g, 81%). ^1H NMR (500 MHz, CDCl_3): δ 8.60 (d, $J = 4.6$ Hz, 1H), 8.10 (d, $J = 8.0$ Hz, 1H), 7.91 (d, $J = 8.0$ Hz, 1H), 7.83 (d, $J = 7.6$ Hz, 1H), 7.77 (s, 1H), 7.68–7.60 (m, 2H), 7.38 (t, $J = 7.4$ Hz, 1H), 7.24–7.13 (m, 7H), 6.77 (t, $J = 7.4$ Hz, 2H), 6.45 (d, $J = 9.3$ Hz, 2H). ^{13}C NMR (125 MHz, CDCl_3): δ 151.47, 149.65, 136.74, 128.81, 128.58, 127.91, 127.12, 125.84, 124.70, 124.37, 123.47, 122.16, 120.77, 120.39, 116.93, 54.45.

fac-Ir(SFXpy) $_3$. Ir(acac) $_3$ (720 mg, 1.50 mmol) and 2-pyridinyl-9,9'-spirobifluorene (2.04 g, 5.18 mmol) were mixed in glycerol (135 mL) under a nitrogen atmosphere. The reaction mixture was heated at 220 °C for 18 h, after which the mixture was cooled to room temperature and water (150 mL) was added. The resulting mixture was extracted with CH_2Cl_2 (3×100 mL), and the organic phase was dried over MgSO_4 . Upon solvent removal under vacuum, the residue was purified by column chromatography using CH_2Cl_2 as the eluent to afford the title compound as an orange solid (761.8 mg, yield 35%). ^1H NMR (500 MHz, CDCl_3): δ 7.74 (d, $J = 8.3$ Hz, 3H), 7.61 (d, $J = 5.2$ Hz, 3H), 7.51–7.47 (m, 6H), 7.36 (d, $J = 7.6$ Hz, 3H), 7.24–7.21 (m, 12H), 7.17 (dd, $J = 13.4$ and 6.3 Hz, 6H), 7.10 (d, $J = 6.2$ Hz, 6H), 7.03–6.98 (m, 3H), 6.81 (dd, $J = 13.6$ and 7.0 Hz, 6H), 6.71 (t, $J = 7.4$ Hz, 3H), 6.46 (d, $J = 7.8$ Hz, 3H). ^{13}C NMR (125 MHz, CDCl_3): δ 166.43, 161.87, 156.41, 151.70, 151.46, 148.00, 147.22, 144.48, 140.24, 135.82, 128.80, 128.29, 127.89, 126.74, 126.05, 125.35, 123.23, 121.79, 121.32, 120.68, 119.60, 116.69, 53.83. MS (MALDI-TOF): m/z 1417.230 ($[\text{M}^+]$).

X-ray Crystallography. X-ray diffraction data were obtained from a Bruker Smart-1000 CCD diffractometer using graphite-monochromated $\text{Mo K}\alpha$ ($\lambda = 0.71073$ Å) radiation at 295 K. The data were collected using the $\omega/2\theta$ scan mode and corrected for Lorentz and polarization effects as well as absorption during data reduction using *SHELXL-97* software. CCDC 1482495 and 1522839 contain the supplementary crystallographic data of *fac-Ir(SFXpy) $_3$* and SFXpy, respectively. These data can be obtained free of charge from the Cambridge Crystallographic Data Centre via www.ccdc.cam.ac.uk/data_request/cif.

Computational Details. The calculations were performed using the Vienna ab initio simulation package (VASP).⁵⁷ The generalized gradient approximation of Perdew–Burke–Ernzerhof⁵⁸ was adopted for the exchange–correlation functional. The energy cutoff for plane-wave expansion was set to 400 eV. All atoms were allowed relax until the atomic Hellmann–Feynman forces were smaller than 0.02 eV Å⁻¹.

The effect of van der Waals interaction was included by using the D3 correction scheme of Grimme.⁵⁹

OLED Fabrication and Measurements. Dry-Processed OLEDs. All of the devices were fabricated onto prepatterned indium–tin oxide (ITO) with a sheet resistance of 10 $\Omega \square^{-1}$. The substrates were cleaned sequentially with detergent, acetone, ethanol, and deionized water under sonication, then dried in an oven, and finally treated in an ultraviolet–ozone chamber. After organic deposition, 100-nm-thick aluminum was covered directly on the organic layer serving as the cathode. The cathode area defines an active device area of $2 \times 2 \text{ mm}^2$ through a shadow mask. Current–voltage–luminance (J – V – L) characteristics were measured with a PR650 spectrascan spectrometer and a Keithley 2400 programmable voltage–current source. EQE was determined following a reported method.⁶⁰ All of the measurements were carried out in the ambient environment without encapsulation.

Wet-Processed OLEDs. A PEDOT:PSS layer was spin-coated directly onto the precleaned ITO glass at a spin speed of 2000 rpm for 60 s and dried at 120 °C for 20 min under vacuum conditions. *fac-Ir(SFXpy) $_3$* and the host material were dissolved separately in chlorobenzene, from which different weight ratios of *fac-Ir(SFXpy) $_3$* /hosts were prepared. The emissive layer was spin-coated onto the top of the PEDOT:PSS layer and annealed at 100 °C for 20 min to remove residual solvents. TmPyPB, LiF, and the aluminum cathode were vacuum-deposited in order under a pressure lower than 5×10^{-4} Pa. The thicknesses of the organic films were measured using a spectroscopic ellipsometry (α -SE, J. A. Wollam Co. Inc.). The current J – V – L characteristics were measured by a Keithley 2602 sourcemeter with a calibrated silicon photodiode. The EL spectra of the devices were analyzed with a PR655 spectrometer. All device characterizations were carried out under ambient laboratory air at room temperature. The emission area of the devices was 12 mm².

■ ASSOCIATED CONTENT

● Supporting Information

The Supporting Information is available free of charge on the ACS Publications website at DOI: 10.1021/acs.inorgchem.7b01034.

NMR, MS, TGA, and DSC characterization, crystal data of SFXpy and *fac-Ir(SFXpy) $_3$* , and the EL performance of the devices (PDF)

■ Accession Codes

CCDC 1482495 and 1522839 contain the supplementary crystallographic data for this paper. These data can be obtained free of charge via www.ccdc.cam.ac.uk/data_request/cif, or by emailing data_request@ccdc.cam.ac.uk, or by contacting The Cambridge Crystallographic Data Centre, 12 Union Road, Cambridge CB2 1EZ, UK; fax: +44 1223 336033.

■ AUTHOR INFORMATION

■ Corresponding Authors

*E-mail: sunyaguang@syuct.edu.cn.
*E-mail: ccnusbli@mail.cnu.edu.cn.
*E-mail: yliu@lbl.gov.

■ ORCID

Bao-Yi Ren: 0000-0001-5879-3291
Ya-Guang Sun: 0000-0001-5850-0938
Yi Liu: 0000-0002-3954-6102
Wei Huang: 0000-0001-7004-6408

■ Author Contributions

[†]These authors contributed equally to this work.

■ Notes

The authors declare no competing financial interest.

ACKNOWLEDGMENTS

This work was financially supported by the National Natural Science Foundation of China (Grant 21501122), and part of the work was carried out as a user project in the Molecular Foundry, a user facility supported through the Office of Science, Office of Basic Energy Sciences, U.S. Department of Energy, under Contract DE-AC02-05CH11231.

REFERENCES

- (1) Yang, X.; Zhou, G.; Wong, W.-Y. Functionalization of phosphorescent emitters and their host materials by main-group elements for phosphorescent organic light-emitting devices. *Chem. Soc. Rev.* **2015**, *44*, 8484–8575.
- (2) Wong, W.-Y.; Ho, C.-L. Heavy metal organometallic electrophosphors derived from multi-component chromophores. *Coord. Chem. Rev.* **2009**, *253*, 1709–1758.
- (3) Lee, J.; Chen, H.-F.; Batagoda, T.; Coburn, C.; Djurovich, P. I.; Thompson, M. E.; Forrest, S. R. Deep blue phosphorescent organic light-emitting diodes with very high brightness and efficiency. *Nat. Mater.* **2015**, *15*, 92–98.
- (4) Chi, Y.; Chou, P.-T. Transition-metal phosphors with cyclometalating ligands: fundamentals and applications. *Chem. Soc. Rev.* **2010**, *39*, 638–655.
- (5) Sajoto, T.; Djurovich, P. I.; Tamayo, A. B.; Oxgaard, J.; Goddard, W. A.; Thompson, M. E. Temperature Dependence of Blue Phosphorescent Cyclometalated Ir(III) Complexes. *J. Am. Chem. Soc.* **2009**, *131*, 9813–9822.
- (6) Ying, L.; Ho, C.-L.; Wu, H.; Cao, Y.; Wong, W.-Y. White Polymer Light-Emitting Devices for Solid-State Lighting: Materials, Devices, and Recent Progress. *Adv. Mater.* **2014**, *26*, 2459–2473.
- (7) Tang, K.-C.; Liu, K. L.; Chen, I. C. Rapid intersystem crossing in highly phosphorescent iridium complexes. *Chem. Phys. Lett.* **2004**, *386*, 437–441.
- (8) Takayasu, S.; Suzuki, T.; Shinozaki, K. Intermolecular interactions and aggregation of *fac*-tris(2-phenylpyridinato- C^2,N)iridium(III) in nonpolar solvents. *Phys. Rev. B* **2013**, *117*, 9449–9456.
- (9) Wehrmeister, S.; Jäger, L.; Wehlus, T.; Rausch, A. F.; Reusch, T. C. G.; Schmidt, T. D.; Brütting, W. Combined electrical and optical analysis of the efficiency roll-off in Phosphorescent organic light-emitting diodes. *Phys. Rev. Appl.* **2015**, *3*, 024008.
- (10) Baldo, M. A.; Adachi, C.; Forrest, S. R. Transient analysis of organic electrophosphorescence. II. Transient analysis of triplet-triplet annihilation. *Phys. Rev. B: Condens. Matter Mater. Phys.* **2000**, *62*, 10967–10977.
- (11) Zhou, G.; Wong, W.-Y.; Yao, B.; Xie, Z.; Wang, L. Triphenylamine-dendronized pure red iridium phosphors with superior OLED efficiency/color purity trade-offs. *Angew. Chem., Int. Ed.* **2007**, *46*, 1149–1151.
- (12) Xu, H.; Chen, R.; Sun, Q.; Lai, W.; Su, Q.; Huang, W.; Liu, X. Recent progress in metal-organic complexes for optoelectronic applications. *Chem. Soc. Rev.* **2014**, *43*, 3259–3302.
- (13) Lo, S.-C.; Burn, P. L. Development of dendrimers: macromolecules for use in organic light-emitting diodes and solar cells. *Chem. Rev.* **2007**, *107*, 1097–1116.
- (14) Mroz, W.; Ragni, R.; Galeotti, F.; Mesto, E.; Botta, C.; Cola, L. D.; Farinola, G. M.; Giovannella, U. Influence of electronic and steric effects of substituted ligands coordinated to Ir(III) complexes on the solution processed OLED properties. *J. Mater. Chem. C* **2015**, *3*, 7506–7512.
- (15) You, Y.; Park, S. Y. Phosphorescent iridium(III) complexes: toward high phosphorescence quantum efficiency through ligand control. *Dalton Trans.* **2009**, 1267–1282.
- (16) Xie, H. Z.; Liu, M. W.; Wang, O. Y.; Zhang, X. H.; Lee, C. S.; Hung, L. S.; Lee, S. T.; Teng, P. F.; Kwong, H. L.; Zheng, H.; Che, C. M. Reduction of self-quenching effect in organic electrophosphorescence emitting devices via the use of sterically hindered spacers in phosphorescence molecules. *Adv. Mater.* **2001**, *13*, 1245–1248.
- (17) Kim, D. H.; Cho, N. S.; Oh, H.-Y.; Yang, J. H.; Jeon, W. S.; Park, J. S.; Suh, M. C.; Kwon, J. H. Highly efficient red phosphorescent dopants in organic light-emitting devices. *Adv. Mater.* **2011**, *23*, 2721–2726.
- (18) Jung, S. O.; Zhao, Q.; Park, J.-W.; Kim, S. O.; Kim, Y.-H.; Oh, H.-Y.; Kim, J.; Kwon, S.-K.; Kang, Y. A green emitting iridium(III) complex with narrow emission band and its application to phosphorescence organic light-emitting diodes (OLEDs). *Org. Electron.* **2009**, *10*, 1066–1073.
- (19) Kang, D. M.; Kang, J.-W.; Park, J. W.; Jung, S. O.; Lee, S.-H.; Park, H.-D.; Kim, Y.-H.; Shin, S. C.; Kim, J.-J.; Kwon, S.-K. Iridium complexes with cyclometalated 2-cycloalkenyl-pyridine ligands as highly efficient emitters for organic light-emitting diodes. *Adv. Mater.* **2008**, *20*, 2003–2007.
- (20) Liu, Y.; Ye, K.; Fan, Y.; Song, W.; Wang, Y.; Hou, Z. Amidinate-ligated iridium(III) bis(2-pyridyl)phenyl complex as an excellent phosphorescent material for electroluminescence devices. *Chem. Commun.* **2009**, 3699–3701.
- (21) Wong, W.-Y.; Ho, C.-L.; Gao, Z.-Q.; Mi, B.-X.; Chen, C.-H.; Cheah, K.-W.; Lin, Z. Multifunctional iridium complexes based on carbazole modules as highly efficient electrophosphors. *Angew. Chem., Int. Ed.* **2006**, *45*, 7800–7803.
- (22) Tong, B.; Mei, Q.; Wang, S.; Fang, Y.; Meng, Y.; Wang, B. Nearly 100% internal phosphorescence efficiency in a polymer light-emitting diode using a new iridium complex phosphor. *J. Mater. Chem.* **2008**, *18*, 1636–1639.
- (23) Zou, J.; Wu, H.; Lam, C.-S.; Wang, C.; Zhu, J.; Zhong, C.; Hu, S.; Ho, C.-L.; Zhou, G.-J.; Wu, H.; Choy, W. C. H.; Peng, J.; Cao, Y.; Wong, W.-Y. Simultaneous optimization of charge-carrier balance and luminous efficacy in highly efficient white polymer light-emitting devices. *Adv. Mater.* **2011**, *23*, 2976–2980.
- (24) Wong, W. Y.; Zhou, G. J.; Yu, X. M.; Kwok, H. S.; Tang, B. Z. Amorphous diphenylamino-fluorene-functionalized iridium complexes for high-efficiency electrophosphorescent light-emitting diodes. *Adv. Funct. Mater.* **2006**, *16*, 838–846.
- (25) Wu, H.; Zhou, G.; Zou, J.; Ho, C.-L.; Wong, W.-Y.; Yang, W.; Peng, J.; Cao, Y. Efficient polymer white-light-emitting devices for solid-state lighting. *Adv. Mater.* **2009**, *21*, 4181–4184.
- (26) Zhou, G.-J.; Wong, W.-Y.; Yao, B.; Xie, Z.; Wang, L. Multifunctional metallophosphors with anti-triplet-triplet annihilation properties for solution-processable electroluminescent devices. *J. Mater. Chem.* **2008**, *18*, 1799–1809.
- (27) Zhou, G.-J.; Wang, X.-Z.; Wong, W.-Y.; Yu, X.-M.; Kwok, H.-S.; Lin, Z. New platinum(II) complexes as triplet emitters for high-efficiency monochromatic pure orange electroluminescent devices. *J. Organomet. Chem.* **2007**, *692*, 3461–3473.
- (28) Xie, L.-H.; Zhu, R.; Qian, Y.; Liu, R.-R.; Chen, S.-F.; Lin, J.; Huang, W. Spiro-functionalized ligand with supramolecular steric hindrance to control π - π interaction in the iridium complex for high-performance electrophosphorescent devices. *J. Phys. Chem. Lett.* **2010**, *1*, 272–276.
- (29) Yao, J. H.; Zhen, C.; Loh, K. P.; Chen, Z.-K. Novel iridium complexes as high-efficiency yellow and red phosphorescent light emitters for organic light-emitting diodes. *Tetrahedron* **2008**, *64*, 10814–10820.
- (30) Xie, L.-H.; Liu, F.; Tang, C.; Hou, X.-Y.; Hua, Y.-R.; Fan, Q.-L.; Huang, W. Unexpected one-pot method to synthesize spiro[fluorene-9,9'-xanthene] building blocks for blue-light-emitting materials. *Org. Lett.* **2006**, *8*, 2787–2790.
- (31) Zhao, X.-H.; Xie, G.-H.; Liu, Z.-D.; Li, W.-J.; Yi, M.-d.; Xie, L.-H.; Hu, C.-P.; Zhu, R.; Zhao, Q.; Zhao, Y.; Zhao, J.-F.; Qian, Y.; Huang, W. A 3-dimensional spiro-functionalized platinum(II) complex to suppress intermolecular π - π and Pt...Pt supramolecular interactions for a high-performance electrophosphorescent device. *Chem. Commun.* **2012**, *48*, 3854–3856.
- (32) Zhao, J.; Xie, G.-H.; Yin, C.-R.; Xie, L.-H.; Han, C.-M.; Chen, R.-F.; Xu, H.; Yi, M.-D.; Deng, Z.-P.; Chen, S.-F.; Zhao, Y.; Liu, S.-Y.; Huang, W. Harmonizing triplet level and ambipolar characteristics of wide-gap phosphine oxide hosts toward highly efficient and low

driving voltage blue and green PHOLEDs: an effective strategy based on spiro-systems. *Chem. Mater.* **2011**, *23*, 5331–5339.

(33) Fan, C.; Yang, C. Yellow/orange emissive heavy-metal complexes as phosphors in monochromatic and white organic light-emitting devices. *Chem. Soc. Rev.* **2014**, *43*, 6439–6469.

(34) Yang, X.; Xu, X.; Dang, J.-S.; Zhou, G.; Ho, C.-L.; Wong, W.-Y. From mononuclear to dinuclear iridium(III) complex: effective tuning of the optoelectronic characteristics for organic light-emitting diodes. *Inorg. Chem.* **2016**, *55*, 1720–1727.

(35) Jou, J.-H.; Lin, Y.-X.; Peng, S.-H.; Li, C.-J.; Yang, Y.-M.; Chin, C.-L.; Shyue, J.-J.; Sun, S.-S.; Lee, M.; Chen, C.-T.; Liu, M.-C.; Chen, C.-C.; Chen, G.-Y.; Wu, J.-H.; Li, C.-H.; Sung, C.-F.; Lee, M.-J.; Hu, J.-P. Highly efficient yellow organic light emitting diode with a novel wet- and dry-process feasible iridium complex emitter. *Adv. Funct. Mater.* **2014**, *24*, 555–562.

(36) Breu, J.; Stössel, P.; Schrader, S.; Starukhin, A.; Finkenzeller, W. J.; Yersin, H. Crystal structure of *fac*-Ir(ppy)₃ and emission properties under ambient conditions and at high pressure. *Chem. Mater.* **2005**, *17*, 1745–1752.

(37) Brooks, J.; Babayan, Y.; Lamansky, S.; Djurovich, P. I.; Tsyba, I.; Bau, R.; Thompson, M. E. Synthesis and characterization of phosphorescent cyclometalated platinum complexes. *Inorg. Chem.* **2002**, *41*, 3055–3066.

(38) Coleman, A. W.; Eadie, D. T.; Stobart, S. R.; Zaworotko, M. J.; Atwood, J. L. Pyrazolyl-bridged iridium dimers. 2. contrasting modes of two-center oxidative addition to a bimetallic system and reductive access to the starting complex: three key diiridium structures representing short nonbonding and long and short bonding metal-metal interactions. *J. Am. Chem. Soc.* **1982**, *104*, 922–923.

(39) Yang, X.; Feng, Z.; Zhao, J.; Dang, J.-S.; Liu, B.; Zhang, K.; Zhou, G. Pyrimidine-based mononuclear and dinuclear iridium(III) complexes for high performance organic light-emitting diodes. *ACS Appl. Mater. Interfaces* **2016**, *8*, 33874–33887.

(40) Mi, B. X.; Wang, P. F.; Gao, Z. Q.; Lee, C. S.; Lee, S. T.; Hong, H. L.; Chen, X. M.; Wong, M. S.; Xia, P. F.; Cheah, K. W.; Chen, C. H.; Huang, W. Strong luminescent iridium complexes with $\hat{C}N=N$ structure in ligands and their potential in efficient and thermally stable phosphorescent OLEDs. *Adv. Mater.* **2009**, *21*, 339–343.

(41) Janiak, C. A critical account on π - π stacking in metal complexes with aromatic nitrogen-containing ligands. *J. Chem. Soc., Dalton Trans.* **2000**, 3885–3896.

(42) Huang, K.; Wu, H.; Shi, M.; Li, F.; Yi, T.; Huang, C. Reply to comment on 'aggregation-induced phosphorescent emission (AIPE) of iridium(III) complexes': origin of the enhanced phosphorescence. *Chem. Commun.* **2009**, 1243–1245.

(43) Cui, L.-S.; Liu, Y.; Liu, X.-Y.; Jiang, Z.-Q.; Liao, L.-S. Design and synthesis of pyrimidine-based Iridium(III) complexes with horizontal orientation for orange and white phosphorescent OLEDs. *ACS Appl. Mater. Interfaces* **2015**, *7*, 11007–11014.

(44) Dedeian, K.; Djurovich, P. I.; Garces, F. O.; Carlson, G.; Watts, R. J. A new synthetic route to the preparation of a series of strong photoreducing agents: *fac*-tris-ortho-metalated complexes of iridium(III) with substituted 2-phenylpyridines. *Inorg. Chem.* **1991**, *30*, 1685–1687.

(45) Ostrowski, J. C.; Robinson, M. R.; Heeger, A. J.; Bazan, G. C. Amorphous iridium complexes for electrophosphorescent light emitting devices. *Chem. Commun.* **2002**, 784–785.

(46) Tsuboyama, A.; Iwawaki, H.; Furugori, M.; Mukaide, T.; Kamatani, J.; Igawa, S.; Moriyama, T.; Miura, S.; Takiguchi, T.; Okada, S.; Hoshino, M.; Ueno, K. Homoleptic cyclometalated iridium complexes with highly efficient red phosphorescence and application to organic light-emitting diode. *J. Am. Chem. Soc.* **2003**, *125*, 12971–12979.

(47) Yu, X.-M.; Zhou, G.-J.; Lam, C.-S.; Wong, W.-Y.; Zhu, X.-L.; Sun, J.-X.; Wong, M.; Kwok, H.-S. A yellow-emitting iridium complex for use in phosphorescent multiple-emissive-layer white organic light-emitting diodes with high color quality and efficiency. *J. Organomet. Chem.* **2008**, *693*, 1518–1527.

(48) Nazeeruddin, M. K.; Wegh, R. T.; Zhou, Z.; Klein, C.; Wang, Q.; De Angelis, F.; Fantacci, S.; Grätzel, M. Efficient green-blue-light-emitting cationic iridium complex for light-emitting electrochemical cells. *Inorg. Chem.* **2006**, *45*, 9245–9250.

(49) Kanno, H.; Holmes, R. J.; Sun, Y.; Kena-Cohen, S.; Forrest, S. R. White stacked electrophosphorescent organic light-emitting devices employing MoO₃ as a charge-generation layer. *Adv. Mater.* **2006**, *18*, 339–342.

(50) Huang, S.-Y.; Meng, H.-F.; Huang, H.-L.; Chao, T.-C.; Tseng, M.-R.; Chao, Y.-C.; Horng, S.-F. Uniform dispersion of triplet emitters in multi-layer solution-processed organic light-emitting diodes. *Synth. Met.* **2010**, *160*, 2393–2396.

(51) Wang, X.; Zhang, S.; Liu, Z.; Yue, S.; Zhang, Z.; Chen, Y.; Xie, G.; Xue, Q.; Zhao, Y.; Liu, S. Hybrid white organic light-emitting diodes with improved color stability and negligible efficiency roll-off based on blue fluorescence and yellow phosphorescence. *J. Lumin.* **2013**, *137*, 59–63.

(52) Chen, X.; Liao, J.-L.; Liang, Y.; Ahmed, M. O.; Tseng, H.-E.; Chen, S.-A. High-efficiency red-light emission from polyfluorenes grafted with cyclometalated iridium complexes and charge transport moiety. *J. Am. Chem. Soc.* **2003**, *125*, 636–637.

(53) Zhang, S. M.; Yue, S. Z.; Wu, Q. Y.; Zhang, Z. S.; Chen, Y.; Wang, X. H.; Liu, Z. Y.; Xie, G. H.; Xue, Q.; Qu, D. L.; Zhao, Y.; Liu, S. Y. Color stable multilayer all-phosphor white organic light-emitting diodes with excellent color quality. *Org. Electron.* **2013**, *14*, 2014–2022.

(54) Mu, Y.; Zhang, S.; Yue, S.; Wu, Q.; Zhao, Y. High efficiency yellow organic light-emitting diodes with optimized barrier layers. *Solid-State Electron.* **2015**, *114*, 87–89.

(55) Tonnelé, C.; Stroet, M.; Caron, B.; Clulow, A. J.; Nagiri, R. C. R.; Malde, A. K.; Burn, P. L.; Gentle, I. R.; Mark, A. E.; Powell, B. J. Elucidating the spatial arrangement of emitter molecules in organic light-emitting diode films. *Angew. Chem.* **2017**, DOI: 10.1002/ange.201610727.

(56) Kawamura, Y.; Brooks, J.; Brown, J. J.; Sasabe, H.; Adachi, C. Intermolecular interaction and a concentration-quenching mechanism of phosphorescent Ir (III) complexes in a solid film. *Phys. Rev. Lett.* **2006**, *96*, 017404.

(57) Kresse, G.; Furthmüller, J. Efficient iterative schemes for *ab initio* total-energy calculations using a plane-wave basis set. *Phys. Rev. B: Condens. Matter Mater. Phys.* **1996**, *54*, 11169–11186.

(58) Perdew, J. P.; Burke, K.; Ernzerhof, M. Generalized gradient approximation made simple. *Phys. Rev. Lett.* **1996**, *77*, 3865–3868.

(59) Grimme, S.; Antony, J.; Ehrlich, S.; Krieg, H. A consistent and accurate *ab initio* parametrization of density functional dispersion correction (DFT-D) for the 94 elements H-Pu. *J. Chem. Phys.* **2010**, *132*, 154104.

(60) Meerheim, R.; Nitsche, R.; Leo, K. High-efficiency monochrome organic light emitting diodes employing enhanced microcavities. *Appl. Phys. Lett.* **2008**, *93*, 043310.